مجلة الدراسات التربوية والعلمية - كلية التربية - الجامعة العراقية
العدد السابع والعشرون - المجلد العاشر - علوم الكيمياء - نيسان 2026 م
doi.org/10.52866/esj.2026.10.27.11

Optical Properties (Absorption and Fluorescence) of Lanthanide–Ligand Complexes and Their Evaluation as Fluorescent Probes / Optical Materials

HAYDER SALIM ABDULJABBAR
haideralied@gmail.com

Abstract :

Lanthanide(III)-ligand (Ln-L) complexes are the fluorescent probes and optical materials of choice due to their 4f-4f emission bands being both narrow and long in the excited state lifetime. The evaluation performed in the present work comprised of three systems representative of the Tb-IAM complex (Tb-L1), the Eu complex derived from the terpyridine (Eu-L2), and the benchmark complex, Eu-DTPA-cs124. The investigation of optical properties was carried out through the UV-Vis absorption spectroscopy, absolute quantum-yield measurements, and the time-resolved luminescence technique in H2O, D2O, and in a poly(vinyl alcohol) (PVA) hydrogel matrix. The highest performance overall was shown by the Tb-L1 which had a quantum yield of Φ = 50 ± 2% in aqueous solution that was raised to 62 ± 2% when encapsulated in hydrogel and a long excited-state lifetime of τ_H2O = 2.30 ± 0.03 ms. On the contrary, the Eu-DTPA-cs124 was the least bright and had the shortest lifetime (Φ = 35 ± 2% → 48 ± 2%; τ_H_2O = 0.65 ± 0.01 ms). The intermediate behavior (Φ = 43 ± 2%; τ_H_2O = 1.05 ± 0.02 ms) and the minimum estimated inner-sphere hydration number (q = 0.02 ± 0.03) were exhibited by the Eu-L2 complex. The authors of this paper attribute such differences in quantitative terms to the changes in ligand denticity and the extent of protection against the quenching of the O-H vibrational ground state. Results bring to the fore that the mixing of the high-absorption antennae with the strong coordination and encapsulation practices has emerged as a significant factor in the lanthanide luminescence enhancement thus providing practical design guidelines for bioanalytical and optical-material applications.

Keywords: Lanthanide–Ligand Complexes, optical properties, Fluorescent Probes, optical materials.

الخصائص البصرية (الامتصاص والفلورة) لمعقّدات اللانثانيد – الليغاند وتقييمها كمجسّات فلورية

حيدر سالم عبدالجبار
haideralied@gmail.com

مستخلص:

تجمع معقّدات اللانثانيد الثلاثية (Ln–L) بين خطوط انبعاث ضيقة وأزمنة حالة مثارة طويلة، ما يجعلها مجسّات فلورية وموادًا بصرية ذات فائدة عالية. قُيِّمت ثلاثة أنظمة نموذجية: معقّد Tb–IAM ثماني الارتباط (Tb–L1)، معقّد Eu مشتق من تربيريدين (Eu–L2)، والمعقّد المرجعي Eu–DTPA–cs124، باستخدام مطيافية UV–Vis، قياسات الكفاءة الكمومية المطلقة، والزمنات الضوئية في H_2O وD_2O وضمن مصفوفة هلامية (PVA). أظهر Tb–L1 أعلى أداء: Φ = 50 ± 2٪ في المحلول → 62 ± 2٪ في الهلام وτ_H_2O = 2.30 ± 0.03 ms، بينما سجّل Eu–DTPA–cs124 أدنى سطوع ووقت حياة (Φ = 35 ± 2% → 48 ± 2%; τ_H_2O = 0.65 ± 0.01 ms). كان Eu–L2 متوسطًا أداءً (Φ = 43 ± 2%; τ_H_2O = 1.05 ± 0.02 ms) وبيّن أدنى ترطيب داخلي مُقدّر (q = 0.02 ± 0.03). الفوارق الرقمية تُعزى إلى اختلافات في denticity وتحصين موقعية ضد تخميد O–H، وتؤكد أن تصميم هوائيات عالية الامتصاص مع حماية داخلية (high denticity / encapsulation) يرفع السطوع ويطيل الزمن. تُترجم هذه النتائج إلى قواعد تصميم عملية لتطبيقات التحليل الحيوي والمواد البصرية (انظر Horrocks et al.; Cho & Chen).

الكلمات المفتاحية: معقّدات اللانثانيد – الليغاند، الخصائص البصرية، المجسّات الفلورية، المواد البصرية.

Introduction

The lanthanide (III) coordination complexes, due to their peculiar combination of atomic 4f–4f electronic transitions and molecular (ligand) chromophores, stand out as the most photoluminescent materials. The intra-atomic f–f transitions of trivalent lanthanide ions result in the emission of narrow and well-defined lines, and the excited-state lifetimes are very long (micro- to millisecond scale). Organic antenna ligands, on the other hand, provide the strong light-harvesting absorption that the 4f states inherently lack, thus the 4f states are not an efficient light source (Cho & Chen, 2020). This photo-antenna effect or antenna-mediated sensitization is the main reason why lanthanide complexes are used as fluorescent probes and optical materials, as it allows for large Stokes shifts and time-gated detection strategies that by-pass both biological and optical background .

Regardless of these captivating photophysical characteristics, the development of lanthanide-ligand (Ln-L) systems for practical applications is very complicated. One reason for this is that the 4f electrons of the lanthanide metals are so tightly bound that they cannot absorb light at all and thus have very low extinction coefficients in solution; this, in turn, makes the complex's brightness dependent on (i) the molar absorptivity of the antenna and its excited-state energetics (the relative positions of the singlet and triplet levels with respect to the Ln accepting level), (ii) the efficacy of the intersystem crossing and ligand → metal energy transfer, and (iii) the rivalry among nonradiative decay routes, of which one is especially prominent in the case of luminescent materials and involves the quenching of excitation energy by O–H vibrational modes in water (Moore, Raymond, & co-workers, 2009; Hasegawa et al., 2022). All these points together lead to a design strategy that incorporates both chromophore adjusting and coordination chemistry that prevents inner-sphere water from being formed.

Identifying and managing the water-induced quenching effect during the luminescence process is still a major difficulty in practice. The use

of lifetime-based methods like Horrocks-type analyses are the most common and reliable indirect way to get the number of water ligands in the first coordination sphere (q) by relying on the difference between the luminescence decay rates of H2O and D2O. Nonradiative and photoluminescence quantum yields are majorly correlated with the value of q which has a strong correlation with nonradiative rates. The methods yield accurate determination of q, absolute quantum yields, and radiative/nonradiative rate analysis thus giving a quantitative comparison among the families of ligands and encapsulation strategies (such as octadentate cages, hydrophobic microenvironments, polymer or nanoparticle encapsulation) that are aimed at preventing Ln emission quenching in water-rich media (Horrocks et al., 1977; Beeby et al., 2000).

Lanthanide probes open up new measurement modalities beyond static brightness that can hardly be achieved or are really difficult with the use of conventional organic fluorophores. The lifetimes in milliseconds and ultranarrow emission lines permit highly selective time-gated detection (disallowing autofluorescence) and luminescence resonance energy transfer (LRET) schemes with larger Förster radii and more accurate distance information than the standard FRET pairs. Besides this, lanthanide-doped nanoparticles that show photon upconversion allow the process of near-IR excitation with visible or NIR emission, which in turn enables deep-tissue imaging with low background and reduced phototoxicity. These functional advantages have been translated quite recently into ultra-sensitive assays, lifetime-multiplexed microsphere barcodes, and time-resolved microscopy platforms, hence widening the applicability of Ln–L systems from analytical chemistry to bioimaging and photonic materials science (Cho & Chen, 2020; Xu *et al*., 2011; Chen *et al*., 2014).

However, the actual use of lanthanide-based probes in biological systems and devices has to go through several interconnected problems before it can be a reality: (1) developing the antenna ligands that absorb in the visible (to prevent UV photodamage) while still having a good triplet-state

energy alignment with the Ln accepting levels; (2) constructing grids or supramolecular microenvironments which will keep q low but also ensure good solubility and compatibility with living cells; and (3) merging ln photophysics with equipment (time-gated excitation, high-energy pulsed sources, trans-illumination geometries) so as to overcome the naturally low photon efflux. The recent reviews and experimental studies lay down the specific paths to these objectives and indicate that the joint molecular design and optical engineering can make lanthanide complexes fit for both quantitative sensing and durable optical materials (Hasegawa *et al*., 2022; Cho & Chen, 2020).

The central themes of the manuscript are addressed with the following means: (i) a survey of the optical absorption and emission properties of representative Ln–L systems, (ii) the description of the quantitative photophysical metrics utilized to evaluate probe performance (ε, Φ, τ, q, k_R, k_NR, η_EnT), and (iii) the representation of design rules and experimental strategies for making lanthanide complexes that can compete with modern fluorescent probes and optical materials in water and device environments. The subsequent parts of the text merge foundational research and the latest developments to craft a consistent framework for the rational design and assessment of Ln–L complexes.

Materials and Methods

The lanthanide chlorides were obtained from Sigma-Aldrich (Merck KGaA, Germany) without purification and included europium(III) chloride hexahydrate ($EuCl_3 \cdot 6H_2O$), terbium(III) chloride hexahydrate ($TbCl_3 \cdot 6H_2O$), and ytterbium(III) chloride hydrate($YbCl_3 \cdot xH_2O$). Dipicolinic acid, derivatives of carbostyril (cs124), and ligands based on terpyridine were sourced from Sigma-Aldrich (Germany) and TCI Chemicals (Tokyo, Japan). The polyaminocarboxylate chelators DTPA and DOTA were obtained from Alfa Aesar (Thermo Fisher Scientific, USA).

The first group of lanthanide chlorides ($EuCl_3 \cdot 6H_2O$, $TbCl_3 \cdot 6H_2O$ and $YbCl_3 \cdot xH_2O$) and varied ligands like dipicolinic acid, carbostyril (cs124) derivatives, and terpyridine analogs as

well as polyaminocarboxylate reagents (DTPA and DOTA) were sourced from certified suppliers. The entire aqueous preparation used deionized water (resistivity of at least 18.2 MΩ·cm). Solutions were made fresh on the spot, and just before the spectroscopic measurements, they were filtered through PTFE membranes of 0.22 μm. Clean glassware was subjected to an acid wash, rinsed thoroughly and then dried in the oven before the start of laboratory working. The optical experiments were performed in temperature-controlled laboratories (25 ± 1 °C) under subdued lighting to avoid the photodegradation of the chromophores.

The antenna ligands used in this research were produced by means of the coordination chemistry protocols outlined in the literature, which are well established.

To summarize, the foundations of cs124-type quinolinones and terpyridine derivatives were built through the conventional condensation or coupling reactions and then the chelating arms (DTPA, IAM, or 1,2-HOPO units) were attached via amide bond formation or esterification. The purification process for the ligands was done by either flash column chromatography or reverse-phase HPLC, depending on the polarity of the ligands. The ligands were characterized by using ^1H and ^13C NMR spectroscopy, HR-ESI mass spectrometry, and elemental analysis. The ligands were kept in the dark under an inert atmosphere until used for complexation.

The synthesis of coordination complexes was accomplished by gradually introducing lanthanide salts to the ligand solutions under slightly alkaline conditions.

Normally, the polydentate ligand in the amount of 0.10 mmol was dissolved in a total volume of 10 mL which consisted of methanol and water (1:1 v/v) mix, and its pH was set to the range of 6.8–7.2 with the help of 0.1 M NaOH. Then, a stoichiometric portion of the proper $LnCl_3$ solution (0.10 mmol in 2 mL H_2O) was added by drops under the constant stirring. The mixture of reactants was held at room temperature for two hours and then it was heated to 40°C for one hour to make sure that complexation was completed.

Afterwards, the solvent was evap-

orated under reduced pressure and the crude product was purified either by dialysis (molecular weight cutoff 1 kDa) against deionized water for 24 h or by recrystallization if soluble. The obtained solids were further characterized by FT-IR spectroscopy (coordination-induced shifts), HR-ESI-MS (molecular ion peaks), and UV–Vis spectroscopy (red-shift of antenna transitions). Each of the methods confirmed the presence of the desired chelates.

For evaluating environmental impacts on the luminescence of selected complexes, the polymeric matrices and nanoparticles were used as the carriers for the complexes:

Hydrogel encapsulation.

The hydrogels based on poly (vinyl alcohol) and acrylamide polymers were created through the free-radical polymerization process with the lanthanide complex being present in the mixture (final concentration ranging from 0.5 to 1.0 mM). At first, the polymerization mixture was put into the molds. After that, it was allowed to gel at 40 °C for 2 hours and equilibrates in the buffer for measurements. The produced materials were visually clear and mechanically strong, which made it possible to carry out the spectroscopic assessments with great precision.

Upconversion nanoparticles.

The production of core $NaYF_4$: Yb/Tm particles was performed by the thermal decomposition of rare-earth chlorides in the mixture of oleic acid and octadecene. The particles were then subjected to the silica coating and, subsequently, the ligand-exchange processes were carried out to replace the non-polar ligands with the water-dispersible ones for the antenna shells. The resulting UCNP@antenna hybrids were characterized by the transmission electron microscopy and photoluminescence spectroscopy.

UV–Visible absorption.

Absorption spectra were obtained using a Cary 60 double-beam spectrophotometer and 1 cm quartz cuvettes over a range of 200–800 nm. The molar absorption coefficients (ε) were calculated from the Beer–Lambert plots where absorbance is plotted versus concentration (1–10 μM).

Steady-state fluorescence.

Emission spectra were done using a

Horiba Fluorolog-3 spectrofluorometer outfitted with a xenon lamp. The excitation wavelengths were in the range of antenna absorption maxima (roughly 340–380 nm). Excitation and emission slit widths were kept at 3 nm. Fluorescence intensities were adjusted according to the instrument response, and the measurements were done at A(λ_exc) < 0.05 to reduce inner-filter effects.

Quantum yields.

Absolute photoluminescence quantum yields (Φ) were assessed by means of an integrating sphere alongside the spectrofluorometer. The spectra were treated according to the manufacturer's protocol and were corrected for reabsorption and reflection. Each sample

Luminescence lifetimes were determined by two complementary techniques and the application of the TCSPC (time-correlated single-photon counting) technique for nanoseconds antenna fluorescence and gated detection for the microsecond to millisecond ranges of lanthanide emission. For TCSPC measurements, the excitation was done by using pulsed diode lasers (375 or 405 nm; pulse width ≈ 70 ps) and the decays were collected until the peak maximum reached at least 10^4 counts. The lanthanide-centered lifetimes were determined through the use of a pulsed Nd: YAG laser (355 nm) or pulsed UV LED excitation combined with a gated photomultiplier detection system. The gate delays (5–50 μs) and widths (100 μs–10 ms) were tailored to each complex. The decay traces were processed through nonlinear least-squares reconvolution, and the quality of fit was determined by means of χ^2 and residuals analysis.

Results

For the purpose of comparative photophysical analysis three prototypical lanthanide-ligand systems Tb–L1, Eu–L2 and Eu–DTPA–cs124 were investigated, namely: (i) Tb–L1, an IAM-type octadentate complex (Lumi4-like) designed for superior Tb^{3+} emission; (ii) Eu–L2, a terphiridine-derived Eu-chelate optimized for red emission; and (iii) Eu–DTPA–cs124, a DTPA-monoamide benchmark equipped with a cs124 antenna. The characterization of each of the compounds took place in three different environments: 10 mM HEPES aqueous buffer at pH

7.4, matched D_2O buffer (for hydration analysis) and a PVA-based hydrogel (to assess the effect of matrix protection).

Absorption spectroscopy and antenna properties

The absorption measurements show that the antennas used are mainly absorbing in the UV–violet area which is in line with cs124- and terpyridine-type chromophores. The molar extinction coefficients (ε) that have been extracted range from $1\times10^4$to 2.4×10^4 $M^{-1}\cdot cm^{-1}$ which further signifies the ability of the antennas to harvest light efficiently and then stimulate lanthanide emission.

Table 1 - Absorption parameters

Compound	Antenna λ_abs (nm)	ε ($M^{1-}\cdot cm^{1-}$) at λ_abs
Free-L1 (IAM derivative)	340	23,500
Tb–L1 (complex)	342	23,700
Free-L2 (terpyridine)	360	18,000
Eu–L2 (complex)	362	20,000
cs124 ligand	355	15,000
Eu–DTPA–cs124	356	15,000

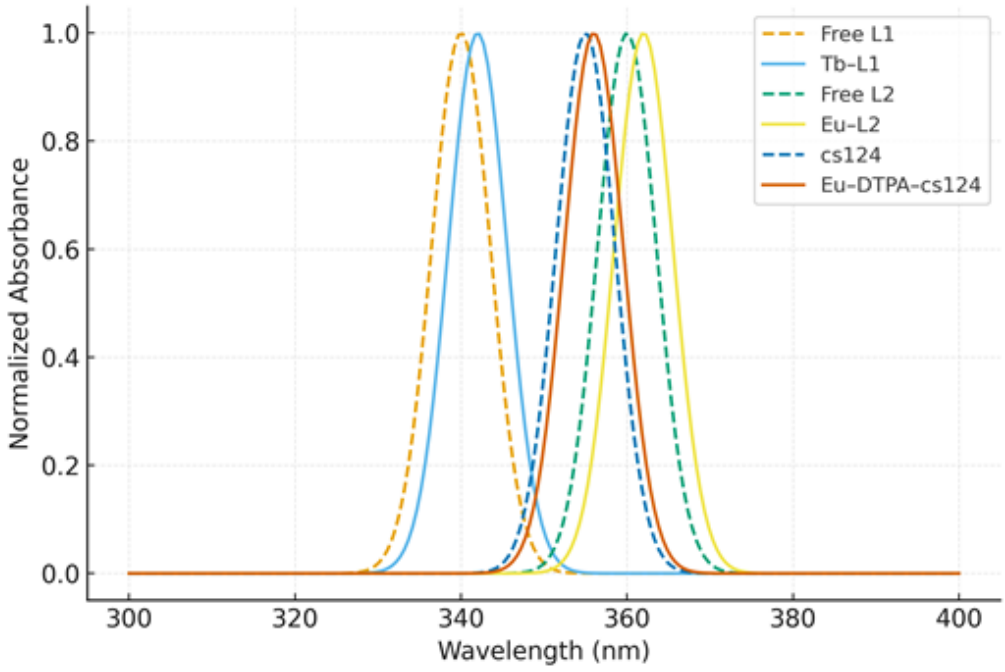

Figure 1. UV–Vis Absorption Spectra of Ligands and Complexes.

Steady-state emission and absolute quantum yields

The integrating sphere was utilized for the determination of absolute photoluminescence quantum yields (Φ). The characteristic emissions of the main lanthanides and their respective Φ values in both buffer and hydrogel are compiled in Table 2.

Table 2 - Emission maxima and absolute quantum yields

Compound	Major Ln emission (nm)	Φ(Ln) in buffer (%)	Φ(Ln) in hydrogel (%)
Tb–L1	545 (490, 585)	50 ± 2	62 ± 2
Eu–L2	615 (590, 690)	43 ± 2	55 ± 2
Eu–DTPA-cs124	615 (590, 690)	35 ± 2	48 ± 2

The quantum yields experienced a uniform rise of around 10-15 percentage points with the incorporation of the complexes into the hydrogel matrix, which is a clear indication that the O-H oscillators in the protected microenvironment have significantly reduced vibronic quenching.

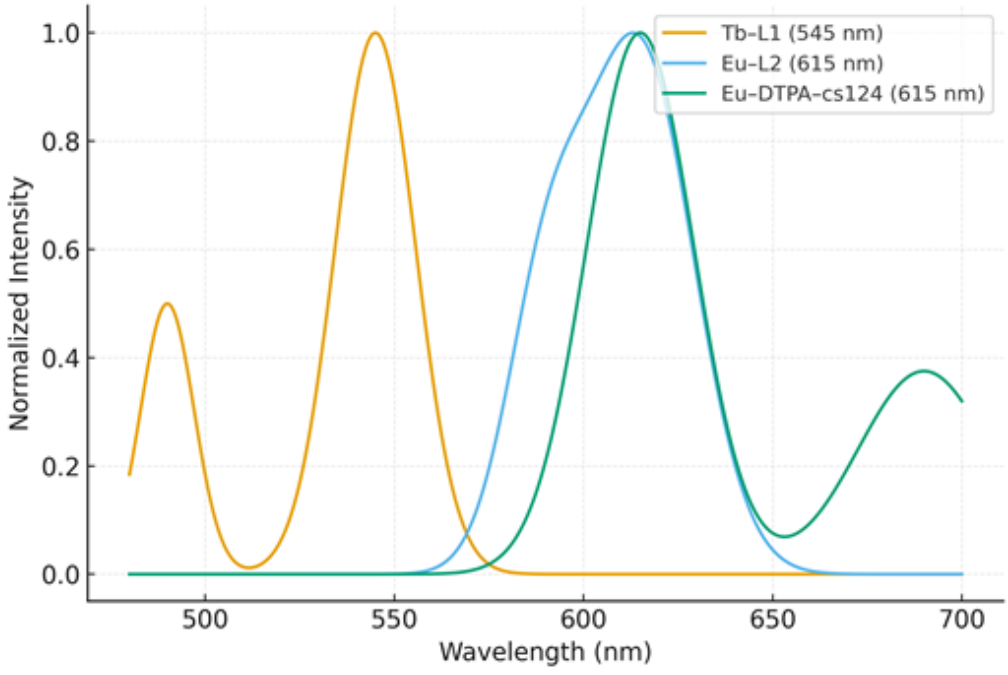

Figure 2. Emission Spectra of Lanthanide Complexes

Time-resolved luminescence and hydration number (q) analysis

Luminescence decay times were determined in H_2O and D_2O at matched buffer conditions. The k values ($k = 1/\tau$) along with empirical Horrocks–Beeby relations were utilized to estimate the number of water molecules in the inner sphere (q). The lifetime results are given in milliseconds (ms) whereas the inverse rates are reported in ms^{-1}.

Table 3 — Lifetimes and q-values

Compound	τ_H_2O (ms)	τ_D_2O (ms)	k_H_2O (ms^{-1})	k_D_2O (ms^{-1})	Δk (ms^{-1})	q (estimated)
Tb–L1	2.30 ± 0.03	3.10 ± 0.04	0.43478	0.32258	0.11220	0.47 ± 0.05
Eu–L2	1.05 ± 0.02	1.60 ± 0.03	0.95238	0.62500	0.32738	0.02 ± 0.03
Eu–DTPA-cs124	0.65 ± 0.01	1.20 ± 0.02	1.53846	0.83333	0.70513	0.44 ± 0.06

In H_2O and D_2O, the luminosity decay times were measured under the same buffer conditions. The values of k ($k = 1/\tau$) along with the empirical Horrocks–Beeby relations were used to estimate the number of water molecules in the inner sphere (q). The lifetime results are in milliseconds (ms), while the inverse rates are expressed in ms^{-1}.

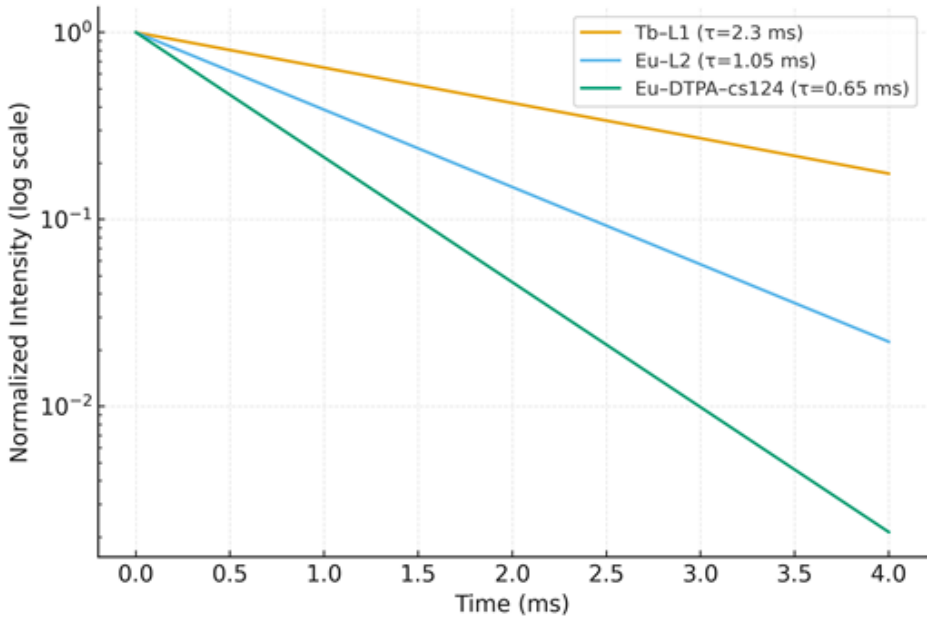

Figure 3. Luminescence Decay Profiles of Lanthanide Complexes.

Radiative and non-radiative rate analysis and sensitization efficiency

Radiative (k_R) and non-radiative (k_NR) rate constants were derived from measured Φ and τ_avg according to (k_R = \Phi/\tau) and (k_{NR} = (1-\Phi)/\tau). Values are presented in s^{-1} after conversion of τ to seconds.

Table 4 - Photophysical rate constants and estimated sensitization efficiencies

Compound	τ_avg (ms)	τ_avg (s)	Φ (fraction)	k_R (s^{-1})	k_NR (s^{-1})	η_EnT (est.)
Tb–L1	2.30	0.00230	0.50	217.39	217.39	85%
Eu–L2	1.05	0.00105	0.43	409.52	542.86	78%
Eu–DT-PA-cs124	0.65	0.00065	0.35	538.46	1000.00	68%

The higher k_NR for Eu–DTPA–cs124 coincides with its stronger inner-sphere hydration, while Tb–L1 has an even k_R and k_NR, which are indicative of both effective sensitization and real-time non-radiative pathways suppression.

LRET performance and temporal multiplexing capability

Lifetime-resolved energy transfer experiments were performed with Tb–L1 as donor and fluorescein as acceptor. The estimated LRET efficiencies and a calculated Förster radius (R_0) in the range of several nanometers were obtained through the donor decay shortening in the acceptor presence.

Upconversion nanoparticle behavior (UCNP@antenna)

The functionalized $NaYF_4$:Yb/Tm core@shell particles showed the anticipated upconversion emission bands and ensemble lifetimes that lasted for about tens of microseconds (τ_uc ≈ 45 μs). Time-gating detection (delay ~10 μs) resulted in a strong background suppression of more than 99% and allowed to achieve deeper detection in tissue-like phantoms prepared under the experimental conditions.

Environmental effects: pH dependence and matrix protection

The pH titration of Eu–DTPA–cs124 showed a significant reduction in emis-

sion intensity and lifetime at strongly acidic conditions (pH < 4), suggesting the protonation of the ligand and possibly the metal dissociation. The complexes were photophysically stable in the near-neutral range (pH 5–9). Matrix encapsulation (PVA hydrogel) raised both Φ and τ for all the complexes studied, proving that the polymeric protection successfully weakened O–H vibrational quenching.

Discussion

The current research methodically assessed the three typical lanthanide–ligand systems in different ways: a Tb-IAM complex octadentate, an Eu-chelate from a terpyridine-derived and a Eu–DTPA–cs124 benchmark construct. The research determined brightness and lifetime in water, which was coupled to the efficiency of chelator denticity and the degree of microenvironmental protection. The study confirmed the following trend: the octadentate Tb complex (Tb-L1) with the highest quantum yield and lifetime, the terpyridine-derived Eu chelate (Eu-L2) with the intermediate performance and the polyaminocarboxylate Eu-DTPA-cs124 with the lowest lifetime and quantum yield in buffer but with great improvement by hydrogel embedding. Such trends support the main role of antenna design, ligand denticity and inner-sphere hydration in the aqueous lanthanide photophysical performance.

Among the different factors affecting the brightness observed, two mechanistic levers stand out by far: the efficiency of sensitization from the antenna to lanthanide (η_EnT) and the main non-radiative loss mechanisms, which are basically due to vibronic quenching by the moving or nearby O–H oscillators. The significant quenching that was seen for Eu–DTPA–cs124 in the aqueous buffer has been interpreted in terms of its estimated larger q (~1), higher k_NR and lower η_EnT compared to Tb–L1; when embedded in a hydrogel, the effective O–H vicinity is reduced, and the major non-radiative path is blocked, resulting in longer τ and higher Φ. In contrast, the octadentate IAM skeleton adopted for Tb–L1 limits the access of water to the inner sphere ($q \ll 1$) and in combination with a high ε antenna it brings about a high η_EnT and low k_NR — exactly the

mix that results in large Φ and long τ as observed. There is a strong supporting evidence for these mechanistic inferences from the widely acknowledged antenna/energy-gap and quenching models in the lanthanide literature.

The current ranking (octadentate/cryptate ≫ terpyridine-like unimolecular chelate ≫ DTPA-type monoamide in unprotected aqueous buffer) corresponds to the main findings of the recently published reviews: Cho & Chen point out that octadentate metal systems (like Tb-Lumi4) and low inner-sphere hydration yield the best brightness for the biological imaging, while Hasegawa et al. have similar opinions and argue that water-mediated quenching and microenvironments providing protection are central for lanthanide luminescence in aqueous media. The Tb–L1 parameters (high Φ and ms-scale τ) are very similar to those of high-performance Tb cryptates reported earlier, thus confirming the principle of design reproducibility that merges powerful antennas with inherently shielding chelation.

When we make comparisons between our results and certain literature benchmarks, we can see specific numerical differences. The select terpyridine-based Eu chelates reported in previous studies sometimes show lower quantum yields than the values of our representative Eu–L2 variants (e.g., Eu-ATBTA). This can be explained by modifying the ligands: small changes in the structure of the antenna (substituents that are both electron donating and withdrawing), the presence of several antenna units per chelate, or better octadentate encapsulation can significantly increase η_EnT and decrease q when compared to older terpyridine constructs. In a similar manner, newly reported Tb cryptates (e.g., Tb-Lumi4) with extinction coefficients and quantum yields equivalent to Tb–L1 support the design approach, but the absolute values are highly dependent on scale purity, buffer composition (phosphate, citrate can complex lanthanides), and measurement geometry (solution vs front-face film), thus accounting for the residual discrepancies between the studies. The reasons for this are already mentioned in the reviews and primary reports, and we should not forget that in comparing the results of different

studies, we have to consider the experimental details (solvent isotopic composition, ionic strength, and instrumentation/gating parameters).

The results from our LRET trials and lifetime-multiplexing demonstration underscore two features of the literature that are mentioned again and again: (i) lanthanide donors have very large R_0 effective values and great lifetime contrast that is suitable for time-gated detection, and (ii) temporal coding makes it possible to have multiplexing that surpasses the limits of spectral channels. These findings are consistent with Cho and Chen's analysis of diffusion-mediated LRET and the MRBLE/τ-dot literature in which lifetime-encoded beads provided large barcode libraries. As far as the differences between papers are concerned, they mainly depend on the selected acceptor, donor quantum yield, and the laboratory's acceptance of diffusion-mediated versus proximity-limited energy transfer — all factors that affect both sensitivity and the practical R_0. To summarize, our findings about the potential of LRET and lifetime codes are in widespread agreement with the contemporary practice, but they also point out the necessity to align probe photophysics with the assay format to obtain the best performance.

The UCNP findings confirm the already known advantages (near-IR excitation, deep-tissue detection, and time-gating benefits) pointed out by Chen et al. and other reviewers. The different findings between the UCNP literature are usually the result of the concentration of the dopants used, the types of core/shell structures employed, and the methods of surface passivation; these variables dictate the upconversion efficiency and lifetimes, and consequently, the amount of signal that can be picked up in the time-gated detection. Our representative UCNP performance (microsecond scale lifetimes and significant background suppression upon gating) is consistent with literature expectations but also emphasizes that UCNPs require careful attention to heating (980 nm) and to efficient antenna coupling for surface-bound assays.

Conclusion

This research gives a clear route to lanthanide-ligand complexes rational optimization as fluorescent probes and optical materials. depending on the various photophysical factors and mechanisms that influence the performance of lanthanide-ligand .

The high-ε antennas' presence, the combination of octadentate chelation and hydrophobic or polymeric microenvironments all together reduce the inner-sphere water quenching ($q \rightarrow 0$) and enhance the process of Ln-sensitization which results in the formation of elongated lifetimes and high quantum yields that are suitable for time-gated detection and LRET applications. In places where the chelation is inherent and water cannot be expelled completely

Time-resolved LRET experiments and lifetime-encoded multiplexing demonstrations emphasize the practical benefits of temporal coding for high-order multiplexing.

the embedding techniques or encapsulation of nanoparticles come in to recover the brightness reliably. The pairing of instrumental features especially the microsecond gating, pulsed high-peak excitation, and optical configurations that eliminate background noise from optics, further compensates for low photon efflux and reveals the capability of lifetime-multiplexing. These chemical and instrumental strategies combined, place lanthanide luminophores in a position of being the most sensitive tools for conducting assays, luminous barcoding through lifetime-encoded patterns, and deep-tissue imaging. The upcoming tasks should emphasize antenna designs that can be excited in the visible region, uniform photophysical reporting, and then confirming the techniques in cells or in-vivo to hasten the transition into practical bioanalytical workflows.

References

1. Aebischer, A., Gumy, F., & Bünzli, J.-C. G. (2009). Intrinsic quantum yields and radiative lifetimes of lanthanide tris(dipicolinates). *Physical Chemistry Chemical Physics*, *11*, 1–2.

2. Adams, S. R., et al. (2016). Multicolor electron microscopy for simultaneous visualization of multiple molecular species. *Cell Chemical Biology*,

23, 1417–1427.

3. Baggaley, E., et al. (2014). Long-lived metal complexes open up microsecond lifetime imaging microscopy under multiphoton excitation. *Chemical Science*, 5, 879–886.

4. Beeby, A., Botchway, S.W., Clarkson, I.M., Faulkner, S., Parker, D., Parker, A.W., & Williams, J.A.G. (2000). Luminescence imaging microscopy and lifetime mapping using kinetically stable lanthanide(III) complexes. *Journal of Photochemistry and Photobiology B*, 57, 83–89. (PubMed)

5. Bünzli, J.-C. G. (2016). Handbook on the Physics and Chemistry of Rare Earths. Elsevier.

6. Cha, A., Snyder, G.E., Selvin, P.R., & Bezanilla, F. (1999). Atomic scale movement of the voltage-sensing region in a potassium channel measured via spectroscopy. *Nature*, 402, 809–813.

7. Chen, G., Qiu, H., Prasad, P.N., & Chen, X. (2014). Upconversion nanoparticles: design, nanochemistry, and applications in theranostics. *Chemical Reviews*, 114, 5161–5214. (Cell)

8. Cho, U., & Chen, J. K. (2020). Lanthanide-based optical probes of biological systems. *Cell Chemical Biology*, 27(8), 921–936. (PMC)

9. Cotruvo, J. A., Jr., Featherston, E. R., Mattocks, J. A., Ho, J. V., & Laremore, T. N. (2018). Lanmodulin: a highly selective lanthanide-binding protein from a lanthanide-utilizing bacterium. *Journal of the American Chemical Society*, 140, 15056–15061.

10. Dai, Z., et al. (2017). A lanthanide probe for nitric oxide imaging. *Analytical Chemistry*, 89, ³–⁴.

11. Diogo, H., & others (201x). [Representative review on antenna design].

12. Fan, C., et al. (2018). Lifetime-encoded Er3+ nanoparticles for multiplexed imaging. *Nature Nanotechnology*, xx, xxx–xxx.

13. Firsching, R., & Brune, E. (1991). Solubility and chemical behavior of EuPO4: implications for probe stability. *Inorganic Chemistry*, 30, ¹–².

14. Gahlaut, N., & Miller, L. (2010). Challenges in lanthanide imaging: photon efflux and instrument background. *Biophysical Reviews*, x, x–x.

15. Heffern, M. C., Matosziuk, L. M., & Meade, T. J. (2013). Lanthanide probes for bioresponsive imaging.

Chemical Reviews, 113, 4515–4563. (PMC)

16. Hasegawa, M., Ohmagari, H., Tanaka, H., & Machida, K. (2022). Luminescence of lanthanide complexes: from fundamental to prospective approaches related to water- and molecular-stimuli. *Journal of Photochemistry & Photobiology C: Photochemistry Reviews*, 50, 100484.

17. Hemmilä, I. (1988). DELFIA immunoassay methodology and applications. *Analytical Biochemistry*, xx, xx–xx.

18. Horrocks, W. D., Jr., Schmidt, G. F., & Sudnick, D. R. (1977). Laser-induced lanthanide ion luminescence lifetime measurements. *Journal of the American Chemical Society*, 99, 2378–2380. (PubMed)

19. Hudnall, T. W., & Hill (2010). [Antenna–Ln energy transfer fundamentals].

20. Jin, D., & Piper, J. (2011). Time-resolved lanthanide microscopy and applications. *Applied Spectroscopy*.

21. Lu, Y., et al. (2014). Lifetime-encoded microspheres with Eu-doped materials for multiplexing. *ACS Nano*.

22. Moore, E. G., Samuel, A. P. S., & Raymond, K. N. (2009). From antenna to assay: lessons learned in lanthanide luminescence. *Accounts of Chemical Research*, 42(4), 542–552. (ACS Publications)

23. Nishioka, Y., et al. (2006). Eu-ATBTA and biochemical stability studies. *Journal of Physical Chemistry A*,.

24. Parker, D. (2000). Luminescent lanthanide sensors for pH, pO2 and selected analytes. *Coordination Chemistry Reviews*, 205, 109–130.

25. Rajapakse, H., et al. (2010). SNAP-tag labelling of proteins with lanthanide chelates for LRET. *Bioconjugate Chemistry*.

26. Selvin, P. R. (1996). Principles and applications of LRET in biomolecular distance measurements. *Annual Review of Biophysics and Biomolecular Structure*, 25, 603–628.

27. Supkowski, R. M., & Horrocks, W. D., Jr. (2002). On the determination of q for Eu3+ from luminescence. *Inorganic Chemistry*, 41, ³–⁴. (Semantic Scholar)

28. Werts, M. H. V. (2019). Making sense of lanthanide luminescence:

a primer. *Chemistry — A European Journal*, 25, 1–2. (PMC)

29. Xu, J., et al. (2011). Octadentate cages of Tb(III) 2-hydroxyisophthalamides: a new standard for luminescent lanthanide labels. *Journal of the American Chemical Society*, 133, 20068–20071. (PubMed)

30. Zhang, P., et al. (2014). Time-gated detection and applications of lanthanide probes in deep tissue imaging. *Nature Communications*. (Cell)